Improved charge separation and transport efficiency in poly(3-hexylthiophene)–TiO_2 nanorod bulk heterojunction solar cells

Chia-Hao Chang, Tse-Kai Huang, Yu-Ting Lin, Yun-Yue Lin, Chun-Wei Chen,* Tsung-Hung Chu and Wei-Fang Su

Received 4th January 2008, Accepted 26th February 2008
First published as an Advance Article on the web 18th March 2008
DOI: 10.1039/b800071a

In this article, we have fabricated photovoltaic devices based on the poly(3-hexylthiophene)–TiO_2 nanorod bulk heterojunction. The microscopic mechanisms of charge separation and charge transport in the poly(3-hexylthiophene)–TiO_2 nanorod nanocomposites have been investigated by photoluminescence quenching, time-resolved photoluminescence spectroscopy, and time-of-flight mobility measurements. Charge separation and transport efficiency can be improved by adding an adequate amount of TiO_2 nanorods in polymer. In addition, the device performance can be further enhanced by thermal annealing or removal of insulating surfactant in the hybrid, giving an optimized device performance of a short circuit current density of 2.62 mA cm^{-2}, an open circuit voltage of 0.69 V, a fill factor of 0.63 under simulated A.M. 1.5 illumination (100 mW cm^{-2}). The corresponding power conversion efficiency under 1 sun is about 1.14%.

1. Introduction

Conjugated polymers have great utility for fabrication of large area, physically flexible and low cost solar cells.[1,2] The performance of photovoltaic devices is largely influenced by two fundamental mechanisms in materials. (i) *Charge separation*—corresponding to the generation of free charge carriers produced by photoexcitation. (ii) *Charge transport*—corresponding to the carriers transported through the device to the electrodes without recombining with oppositely charged carriers. Due to the short exciton diffusion length in a semiconducting polymer[3–5] (<20 nm), the electron acceptors are usually intermixed with polymer at a nanometre length scale to achieve efficient charge separation before recombination. In the past decade, research has been focused on the development of polymer photovoltaic devices, using fullerene or fullerene derivatives as acceptors in combination with a polymer as the donor, and the highest power efficiency conversion rate is about 5%.[2] Alternatively, hybrid polymer solar cells based on conjugated polymers combined with n-type inorganic nanocrystals have been proposed due to the advantage of high electron mobility and excellent chemical and physical stability of inorganic semiconductors. Several polymer–inorganic hybrid solar cells have been reported by using CdSe,[1,6] PbS,[7] TiO_2[8–11] and ZnO[12] nanocrystals respectively. The environmentally friendly and low cost TiO_2 nanocrystal is a promising material in hybrid organic–inorganic photovoltaic device applications. Two of the most common ways that have been used to prepare the hybrid polymer–TiO_2 solar cells are: (i) blending the TiO_2 nanocrystals with polymer by forming the bulk heterojunction[8,9] or (ii) infiltrating the polymer into the porous TiO_2 nanostructures.[10,11] For the hybrid solar cell based on the polymer–porous TiO_2 nanostructure, well connected transport paths can be formed in the semiconductor layer. However, the number of interfaces is still limited by the dimension of the TiO_2 nanostructure. In contrast, the polymer-based bulk heterojunction (BHJ) solar cell, consisting of an electron accepting network formed randomly within the polymer matrix, provides a large number of interfaces for charge separation, but at the expense of poorly formed conducting pathways. Thus, an enhanced charge transport route by using one-dimensional semiconductor nanorods instead of nanoparticles is preferable for offering direct pathways to achieve more efficient electrical conduction. Huynh *et al.* have demonstrated high performance solar cells by combining CdSe nanorods with a better hole transporting mobility polymer, poly(3-hexylthiophene) P3HT.[1] In this article, the environmentally friendly, all-solution processible P3HT–TiO_2 nanorod bulk heterojunction solar cells are studied. The microscopic mechanisms of charge separation and transport in hybrid solar cells based on P3HT–TiO_2 nanorod bulk heterojunctions are investigated by photoluminescence (PL) quenching, time-resolved photoluminescence (TRPL) spectroscopy, photoluminescence excitation spectroscopy (PLE) and time-of-flight (TOF) mobility measurements. In addition, the performance of the photovoltaic device can be further improved by thermal annealing or removal of the insulating surfactant in the hybrid, and the corresponding optoelectronic properties of nanocomposites are also reported.

2. Materials preparation and experimental setup

High aspect ratio anatase titanium dioxide nanorods were synthesized by the hydrolysis of titanium tetraisopropoxide according to literature with modification.[9,13] Typically, oleic acid (O.A.) (120 g, Aldrich, 90%) was stirred vigorously at 120 °C for 1 h in a three-neck flask under Ar flow, then allowed to cool to 90 °C and maintained at this temperature. Titanium isopropoxide (17 mmole, Aldrich, 99.999%) was then added to the flask. After stirring for 5 min, trimethylamine-*N*-oxide

Department of Materials Science and Engineering, National Taiwan University 106, Taiwan. E-mail: chunwei@ntu.edu.tw

dihydrate (34 mmole, ACROS, 98%) in 17 ml water was rapidly injected. The trimethylamine-*N*-oxide dihydrate was used as a catalyst for polycondensation. The reaction was continued for several hours to allow complete hydrolysis and crystallization. The product was washed and precipitated by ethanol repeatedly to remove residual surfactant. Subsequently, the TiO_2 nanorods were collected by centrifugation and then redispersed in toluene. The hybrid materials were prepared by adding an appropriate amount of TiO_2 nanorods into P3HT ($M_w \approx 58\,000$, PDI 1.62, RR 96%) polymer solution to make P3HT–TiO_2 nanorod composite samples. For ligand exchange, firstly, the as synthesized O.A. end-capped TiO_2 nanorods were washed with ethanol three times to remove the oleic acid. Then, the TiO_2 nanorods were dispersed in pyridine and left under stirring at 70 °C until the solution turned clear. Through these procedures, the O.A. (original surface ligand) was removed and the pyridine of a weak binding ligand was on the surface of TiO_2 nanorods, which can be removed through heating.

The TiO_2 nanorod microstructure was measured by a JEOL-2000FX (Japan) transmission electron microscope (TEM) operated at 200 keV. The film morphology was observed by atomic force microscopy (AFM) (Digital Instruments, Nanoscopes III). UV-Vis absorption spectra were obtained using a Jasco V-570 UV/Vis/NIR Spectrophotometer. The steady state PL spectra were taken by the FluoroLog®-3 spectrofluorometer (Jobin-Yvon). Time-resolved photoluminescence (TRPL) spectroscopy was performed with a time-correlated single photon counting (TCSPC) spectrometer (Picoquant, Inc.). A pulse laser (470 nm) with an average power of 1 mW operating at 40 MHz with a duration of 70 ps was used for excitation. For the time-of-flight (TOF) mobility measurements, thick films (several μm) were prepared by drop-casting the P3HT–TiO_2 nanorod blended solutions on the glass substrates, precoated with semi-transparent aluminum electrodes (35 nm) by thermal evaporation at a vacuum about 1×10^{-6} torr. The measured samples were then completed by thermal evaporation of thicker aluminum cathodes (~200 nm) through a shadow mask. For the TOF transient photocurrent measurements, a thin layer of charge carriers were generated under illumination through the semi-transparent electrode using a frequency-doubled Nd:YAG pulsed laser ($\lambda = 532$ nm). The intensity of the incident laser power was kept small enough to avoid accumulation of the photoexcitation charge, which could change the internal electric field. Under the applied electric field, these carriers drifted toward the counter electrode, giving the transient photocurrent signal recorded by a digital oscilloscope (Tetronix TDS5052B). The carrier types (electron or hole) under study was selected by changing the polarity and magnitude of the applied electric field using a Keithley 2410 source meter. The samples were mounted in a vacuum chamber under 1×10^{-3} torr during measurement. For the photovoltaic device fabrication, a 40 nm thick layer of poly (3,4-ethylenedioxythiophene):poly(styrenesulfonate) (PEDOT:PSS) (Baytron P 4083) was spin-cast onto the indium tin oxide (ITO) substrate at 300 rpm for 10 s and 6000 rpm for one minute, followed by baking at 120 °C for 30 min. A thin active P3HT–TiO_2 nanorods hybrid layer with a thickness of about 120 nm was deposited by using spin coating under 1000 rpm for a minute. The Al electrode was then deposited onto the active layer by thermal evaporation under vacuum at a pressure of around 2×10^{-6} Torr. Typical device area was about 0.1 cm^2. Current–voltage measurements (Keithley 2410 source meter) were obtained by using a solar simulator (Newport Inc.) with the A.M. 1.5 filter under an irradiation intensity of 100 mW cm^{-2}. The film thickness was measured by means of a Veeco M6 surface profiler.

3. Result and discussion

3.1 Structure and morphology

The TEM image of TiO_2 nanorods before being blended with P3HT in Fig. 1(a) reveals that the dimensions of the TiO_2 nanorods are 20–40 nm in length and 4–5 nm in diameter. The inset in Fig. 1(a) exhibits the high-resolution TEM (HRTEM) image and the corresponding selected-area diffraction pattern (SADP) of TiO_2 nanorods. The *d*-spacing of this ring pattern is 3.54 Å, 2.39 Å, 1.90 Å and 1.69 Å from inner ring to outer ring, which can be indexed for (101), (004), (200) and (211) of the TiO_2 anatase phase, consistent with the XRD results as shown in Fig. 1(b). The filtered image in the square region indicates that the growth direction of TiO_2 nanorods is along the longitudinal [001] direction in synthesized condition. Fig. 2(a), (b) and (c) represent the atomic force microscopy (AFM) height images of the pristine P3HT and hybrid films. The images clearly show that the addition of TiO_2 nanorods increases the roughness of the films with a larger agglomerate form, showing a root-mean-square (rms) roughness of 2.2 nm, 9.4 nm and 15.7 nm for the samples consisting of 0, 30 and 60 wt% TiO_2 nanorods respectively.

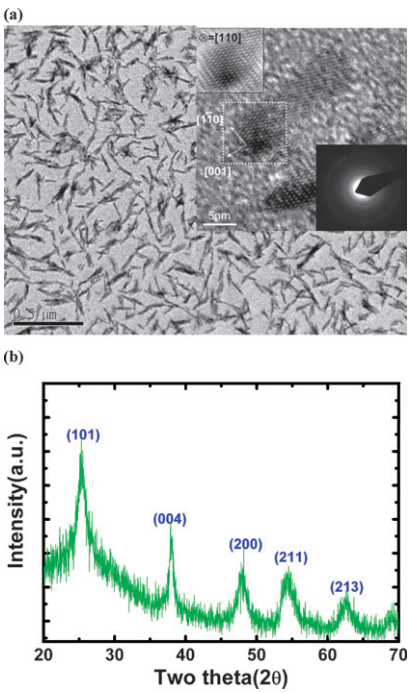

Fig. 1 (a) The TEM image of TiO_2 nanorods. The inset shows the high-resolution TEM (HRTEM) image and the corresponding selected-area diffraction pattern (SADP) of TiO_2 nanorods. (b) X-Ray diffraction (XRD) pattern of TiO_2 nanorods.

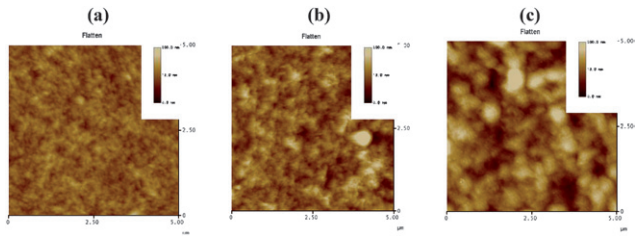

Fig. 2 Tapping-mode AFM topography images taken from the P3HT–TiO_2 nanorod hybrid materials consisting of 0 wt%, 30 wt%, and 60 wt% TiO_2 nanorods respectively. The scanning rage is 5 μm × 5 μm and the scale bar for the height is 100 nm.

3.2 Charge separation and transport in hybrid

Fig. 3(a) shows the UV-vis absorption spectra of the nanocomposites consisting of 0, and 30, 50 and 60 wt% TiO_2 nanorods respectively. The pristine P3HT exhibits a broad absorption spectrum ranged from 400–650 nm and TiO_2 nanorods have an absorption edge at about 350 nm. The optical density of the absorption spectra in the hybrid is simply the sum of the absorption spectra of the constituent parts. In contrast, the yield of the PL emission decreases with the increasing TiO_2 nanorod content as shown in the inset of Fig. 3(a), suggesting the occurrence of photoinduced electron transfer from P3HT to TiO_2 nanorods. The presence of photoinduced charge transfer at the P3HT–TiO_2 nanorod interfaces can be further evident from time-resolved photoluminescence spectroscopy. Fig. 3(b) shows the PL decay curves for the pristine P3HT and the hybrid films respectively. The addition of TiO_2 nanorods in polymer results in a new relaxation process, which provides the donor a further non-radiative process and leads to the enhancement of the non-radiative decay rate. The measured PL decay lifetime for the pristine P3HT and hybrids consisting of 30 50, and 60 wt% TiO_2 nanorods are 720 ps, 580 ps, 520 ps and 470 ps respectively. This produces a charge separated state with an electron on the TiO_2 nanorods and a hole on the polymer. As the content of TiO_2 nanorods in the hybrid is increased, the efficiency of charge separation at the polymer–nanocrystals is enhanced, resulting in shortening of the measured lifetime τ_{PL} and quenching of the PL efficiency. A schematic representation of the mechanism of charge transfer at the P3HT–TiO_2 nanorod interfaces is shown in the inset of Fig. 3(b).

Next, the mechanism of charge transport in the P3HT–TiO_2 nanorod hybrids is investigated by the TOF method. Fig. 4(a) and (b) show the signals of typical hole and electron transient photocurrent of the pristine P3HT respectively. The drift mobility at an applied electric field E, is deduced according to $\mu = d/Et_{tr}$, where d is the thickness of the film, $t_{tr}$is the transit time for the arrival of carriers at the collecting electrode. The hole and electron transient photocurrent for the pristine P3HT is highly dispersive and the transit time t_{tr} can be estimated from the intersection point in the double-logarithmic plot (inset). The calculated hole and electron mobilities for the pristine P3HT are $\mu_h = 2.9 \times 10^{-4}$ cm^2 V^{-1} s^{-1} at $E = 6.0 \times 10^4$ V cm^{-1} and $\mu_e = 1.5 \times 10^{-4}$ cm^2 V^{-1} s^{-1} at $E = 3.0 \times 10^5$ V cm^{-1}, which is very similar to the previous report on the TOF measurement on

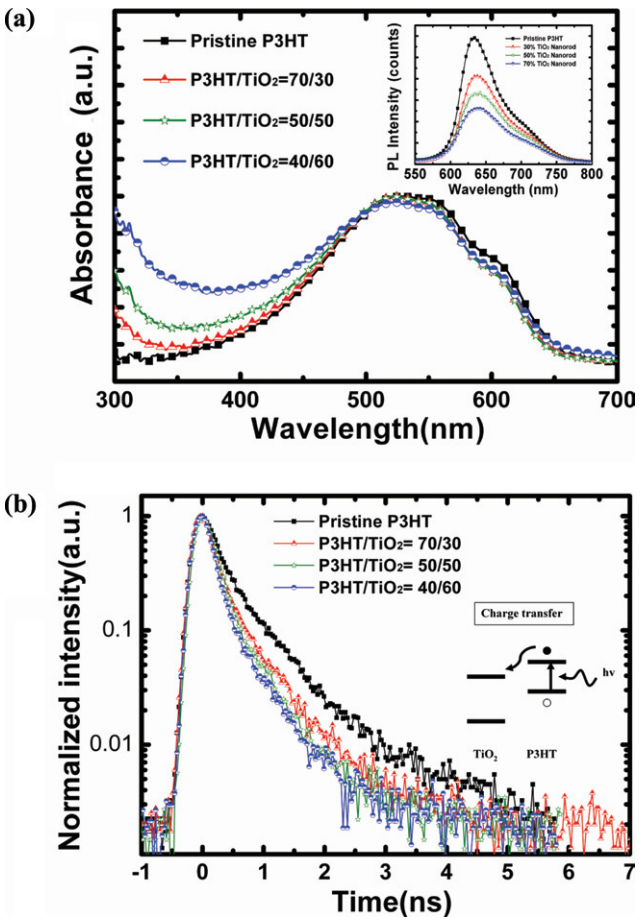

Fig. 3 (a) UV-vis absorption spectra of the P3HT–TiO_2 nanorod hybrid materials consisting of 0 wt%, 30 wt%, 50 wt% and 60 wt% TiO_2 nanorods respectively. The inset shows the corresponding PL yield of the hybrids. (b) Time-resolved PL spectroscopy of the hybrid materials.

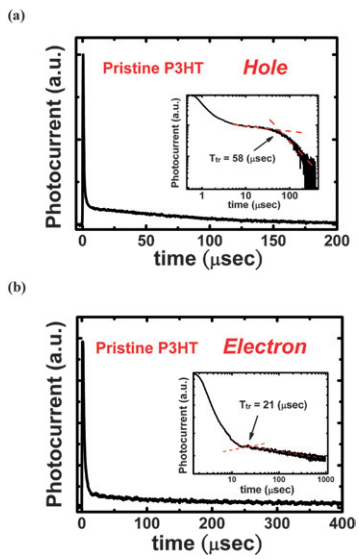

Fig. 4 Typical TOF (a) hole and (b) electron transient photocurrent for pristine P3HT. The insets show the double-logarithmic plots for the transient photocurrent. The thickness for the pristine P3HT thin films is about 10 μm.

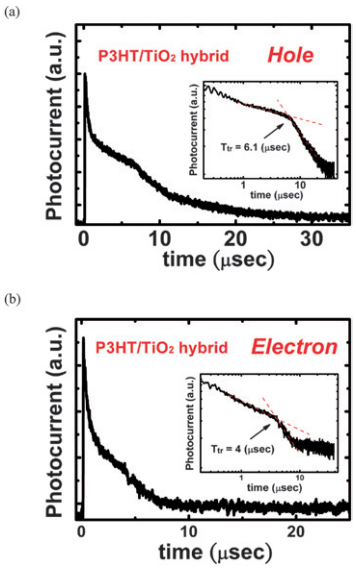

Fig. 5 Typical TOF (a) hole and (b) electron transient photocurrent for P3HT–TiO_2 nanorod hybrid (50 wt%). The insets show the double-logarithmic plots for the transient photocurrent. The thickness of the hybrid film is about 9.7 μm.

pristine P3HT.[14] In contrast, the corresponding hole and electron transient photocurrent for the P3HT–TiO_2 nanorod hybrid consisting of 50 wt% TiO_2 nanorods become less dispersive with a clearly defined plateau region followed by a tail in the decay of the current as shown in Fig. 5(a) and (b). The hole and electron mobilities for the hybrid are evaluated about $\mu_h = 4.4 \times 10^{-3}$ cm^2 V^{-1} s^{-1} at $E = 3.3 \times 10^4$ V cm^{-1} and $\mu_e = 3.5 \times 10^{-3}$ cm^2 V^{-1} s^{-1} at E=5.26 $\times$ 10^4 V cm^{-1} respectively. In general, the photocurrent profile with a less dispersive (or non-dispersive) characteristic in the polymer indicates that the carriers transport through a more ordered structure.[15] The transition from highly dispersive to less dispersive transport behavior indicates that more efficient carrier transport can be achieved after adding an adequate amount of TiO_2 nanorods within the P3HT matrix. The field dependence of the mobility can provide further information on the carrier transport mechanism. Fig. 6(a), (b) and (c) show the field dependence of the hole and electron mobilities of pristine P3HT and P3HT–TiO_2 nanorod hybrids with various concentrations respectively. The mobility data are plotted as a function of the square root of electric field ($\sqrt{E}$)according to the Poole–Frenkel relation[14] of $\ln\mu = s\sqrt{E}$, where the slope s is a slope parameter. For the pristine P3HT, a very weak dependence on the electric field for the mobilities of electrons and holes can be seen, which represent a similar manner to the previous TOF report on the pristine P3HT both in the magnitude and field-independent characters.[14] For the P3HT–TiO_2 nanorod hybrid materials, it is found that both electron and hole mobilities are enhanced with increasing TiO_2 nanorod concentrations up to 50 wt% with a weak electric field dependence. It is worth noting that the relatively lower electric field used in measuring the hybrid samples compared to the pristine sample is mainly due to the increased dark conductivity, which causes difficulty in the extraction of the signal at high electric field. However, estimated from the operation condition of the polymer–TiO_2

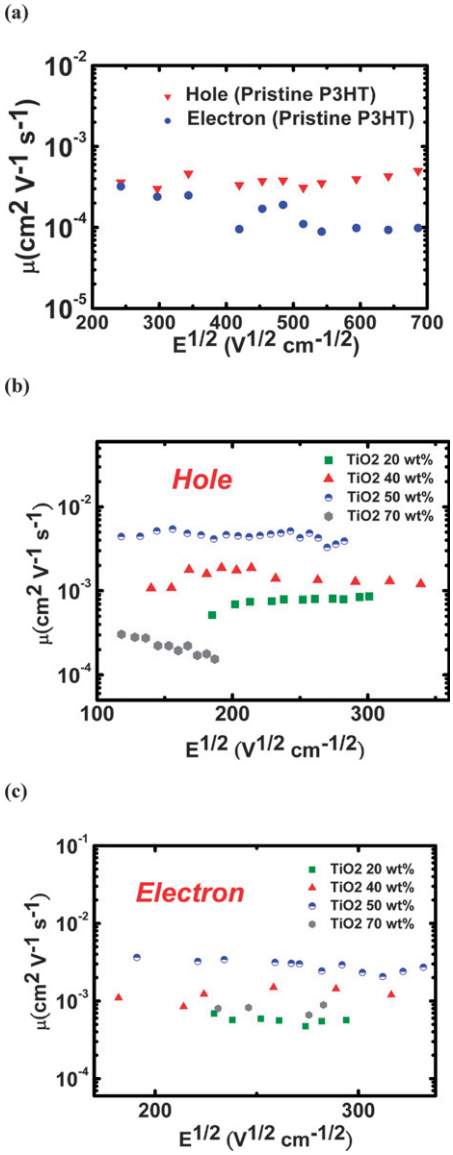

Fig. 6 Field dependence of the (a) hole and electron mobilities for pristine P3HT. Field dependence of the (b) hole and (c) electron mobilities for hybrid samples with different compositions.

nanorod hybrid photovoltaic device at short circuit current, the evaluated electric field is about $E = 4 \times 10^4$ V cm^{-1}, (the open circuit is about 0.6 V and the film thickness is about 150 nm), which is similar to the range in our measurement. Intuitively, the increase in electron mobility after adding TiO_2 nanorods within the polymer matrix is mainly due to the formation of the interconnecting network by TiO_2 nanorods, which can provide more efficient transport pathways for electrons after charge separation. Surprisingly, the enhancement of hole mobility upon adding an adequate amount of TiO_2 nanorod content within the polymer matrix is observed, accompanied by a less dispersive or relatively non-dispersive transport behavior. Tuladhar *et al.* in ref. 16 have also found the enhancement in hole mobility after adding PCBM nanocrystals into the polymer matrix. They proposed that PCBM may assist hole transport in the hybrid, either by participating in hole transport or by changing the polymer chain packing so that hole transport

within the polymer can be accelerated. It is believed that this effect could be also significant in the polymer–TiO_2 nanorod hybrid system at an adequate amount of TiO_2 nanorods up to 50 wt%. For concentrations of TiO_2 nanorods larger than 50 wt%, the hole mobility starts to decline. The slope s of field-dependent hole mobility at a concentration of 70 wt% TiO_2 nanorods even becomes negative, which may be due to (i) the occurrence of large-scale phase segregation in morphology; (ii) the fact that the hole transport in the hybrid is now "blocked" by the appearance of a large number of TiO_2 nanorods. When it can progress further, it must hop *against* the field direction, and the process therefore becomes slower as the field is increased. Therefore, by the inclusion of an adequate amount of TiO_2 nanorods in the polymer, both hole and electron transport can be enhanced, accompanied by less dispersive transport behavior.

3.3 Device performance

The photovoltaic device structure consisting of ITO/PEDOT:PSS/P3HT:TiO_2 nanorod hybrid/ TiO_2 nanorods/Al is shown in Fig. 7(a). An additional layer of TiO_2 nanorods sandwiched between the active hybrid layer and the aluminum electrode was included to act as a hole blocking layer.[9] It has been known that the device performance strongly depends on morphology, charge separation and transport efficiency and interfacial contact.[17,18] The current–voltage characteristics of the devices based on the hybrids with various TiO_2 nanorod contents are also shown in Fig. 7(b). It is found that the device performance is improved with increasing TiO_2 nanorod content up to 50 wt%. Further increasing the TiO_2 nanorods content up to 70 wt% results in a significant decrease in the device performance, consistent with the observed transport behavior. The optimized performance of the device consisting of 50 wt% TiO_2 nanorods shows a short circuit current density (J_{sc}) of 0.91 mA cm^{-2}, an open circuit voltage (V_{oc}) of 0.58 V, a fill factor (FF) of 0.32, and a power conversion efficiency (η) of 0.17%. We have further carried out thermal annealing treatment to enhance

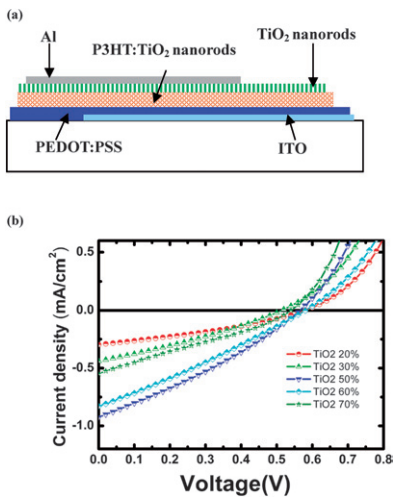

Fig. 7 (a) Schematic representation of the photovoltaic device based on the hybrid material, consisting of ITO/PEDOT:PSS/P3HT–TiO_2 nanorod hybrid/TiO_2 nanorods/Al. (b) Current–voltage characteristics for the P3HT–TiO_2 nanorod hybrid photovoltaic devices with different compositions [under simulated A.M. 1.5 illumination (100 mW cm^{-2})].

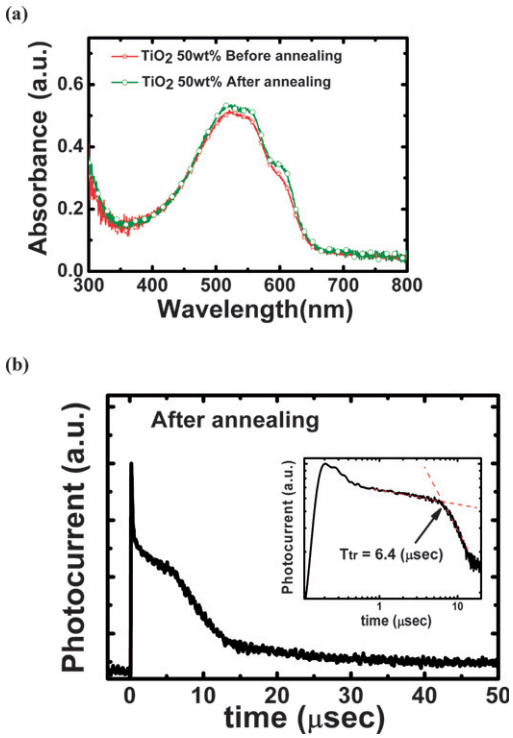

Fig. 8 (a) Optical absorption spectra of the hybrid samples before and after thermal annealing. (b) The transient hole photocurrent of the hybrid sample with 50 wt% TiO_2 nanorod concentration after thermal treatment. The film thickness is about 11 μm.

the device performance by improving the crystallinity of the polymer film.[2,17] Fig. 8(a) shows the UV-vis optical absorption spectra of the P3HT–TiO_2 nanorod hybrids before and after thermal annealing at 110 °C for 0.5 hr. The more pronounced 0–0 and 0–1 vibronic absorption shoulders in the annealed samples are found, indicating the formation of more electronically ordered P3HT chains. The enhanced electronic ordering after thermal annealing can be further supported from the TOF measurement. Fig. 8(b) shows the transient photocurrent signals of hole transport for the P3HT–TiO_2 nanorod hybrid material (TiO_2 = 50 wt%) after the same annealing conditions. Compared to the sample before annealing in Fig. 5(a), the transient hole photocurrent of the annealed sample shows a relatively non-dispersive decay with a more clearly defined plateau region. The value of hole mobility in the hybrid after thermal annealing is increased to 9.0×10^{-3} cm^2 V^{-1} s^{-1} at E=2.0×10^4 V cm^{-1}. Fig. 9 exhibits the photovoltaic device performance of the annealed sample with respect to the as-cast sample. A considerable improvement in the power conversion efficiency up to 0.42% is observed after thermal annealing, giving a short circuit current density (J_{sc}) of 1.79 mA cm^{-2}, an open circuit voltage (V_{oc}) of 0.59 V, and a fill factor (FF) of 0.40.

3.4 Removal of insulating surfactant by ligand exchange

Although improved charge separation and transport efficiency can be achieved after adding TiO_2 nanorods in polymer, the device performance can be still limited by the presence of residual insulating surfactant of oleic acid (O.A.) on the TiO_2 nanorods' surface, leading to a higher serial resistance and

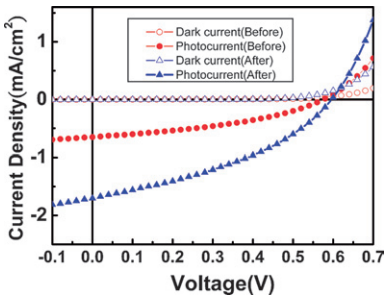

Fig. 9 The dark and photocurrent of the samples before and after thermal annealing.

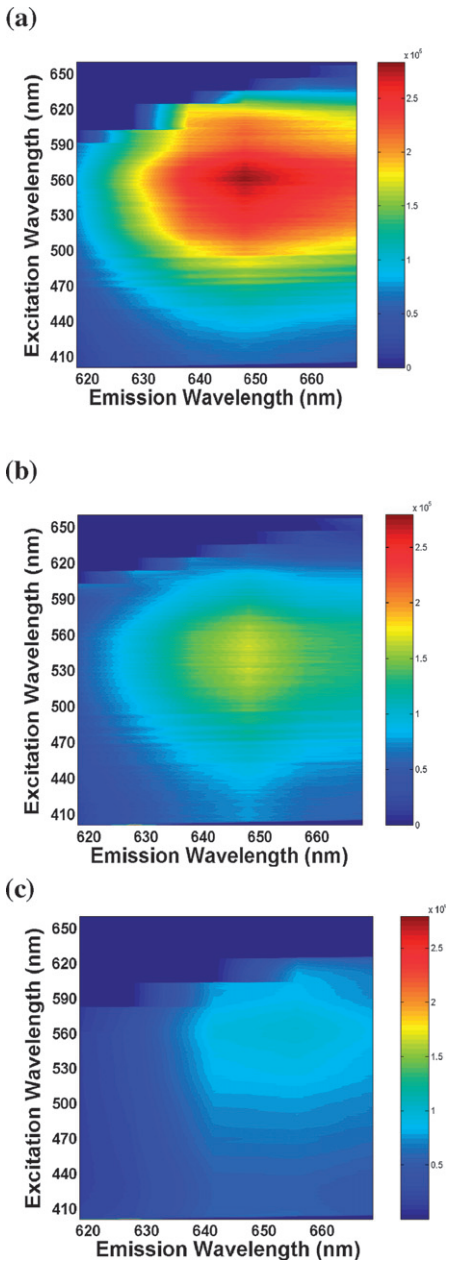

Fig. 10 The two-dimensional PL contour plots for the (a) pristine P3HT, (b) P3HT–TiO_2 nanorod (O.A.) hybrid and (c) P3HT–TiO_2 nanorod (pyridine) hybrid thin films with a similar thickness of about 200 nm.

a lower fill factor. Further improvement in the device performance can be achieved by removing the possible residual surfactant or replacing it with a more conductive surfactant at the P3HT–TiO_2 nanorod interfaces. We have therefore carried out ligand exchange processes to remove the residual surfactant of oleic acid (O.A.) through pyridine treatment according to the literature.[18,19] Through these procedures, the O.A. (original surface ligand) can be removed and the pyridine of a weak binding ligand is on the surface of the TiO_2 nanorods, which can be removed through heating. As shown in Fig. 10(a), (b) and (c), the two-dimensional PL contour plots for the pristine P3HT, P3HT–TiO_2 nanorod (O.A.) hybrid and P3HT–TiO_2 nanorod (pyridine) hybrid thin films are present. The excitation wavelengths ranged from 400–650 nm and almost represent the whole absorption spectral range of P3HT. It is found that the intensity of the PLE signals quenches at all emission wavelengths for both hybrid samples. A much higher quenching efficiency of the P3HT–TiO_2 nanorod (pyridine) hybrid material is found compared to that in the P3HT–TiO_2 nanorod (O.A.) hybrid sample, indicating that more efficient charge separation occurs by removing the possible residual insulating surfactant at the P3HT–TiO_2 nanorods' interfaces. By following similar device fabrication conditions as described above, the photovoltaic device based on the P3HT–TiO_2 nanorod hybrid after pyridine treatment shows a short circuit current density (J_{sc}) of 2.62 mA cm^{-2}, an open circuit voltage (V_{oc}) of 0.69 V, a fill factor (FF) of 0.63, and a power conversion efficiency (η) of 1.14% as shown in Fig. 11. A large increase in the fill factor indicates that removal of insulating surfactant on the TiO_2 nanorods can result in a significant reduction of the serial resistance of the device. The increase in the open circuit voltage V_{oc} after pyridine treatment may be attributed to changes in interfacial dipoles, leading to a shift in the band offset at the TiO_2–polymer interface.[20] In addition, the increase in the open circuit voltage V_{oc} may be also attributed to the reduction of back charge recombination[21] due to interface modification, which may increase the position of the quasi-Fermi level and open circuit voltage. Removal of the insulating surfactant at the P3HT–TiO_2 nanorod interfaces can lead to direct contact between polymer and TiO_2 nanorods, resulting in a further improvement in charge separation and transport efficiencies and giving a higher device performance.

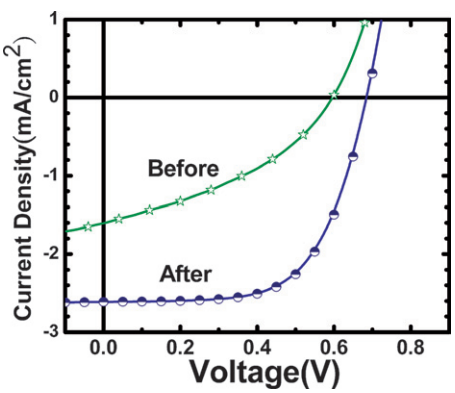

Fig. 11 (a) Photovoltaic performances of the devices under simulated AM 1.5 illumination (100 mW cm^{-2}) before and after removal of insulating surfactant by pyridine treatment.

4. Conclusion

In conclusion, the microscopic mechanisms of charge separation and charge transport in the P3HT–TiO_2 nanorod hybrid have been investigated. Improved charge separation and transport efficiency can be achieved by adding an adequate amount of TiO_2 nanorods in polymer, or through thermal annealing and removal of insulating surfactant. The results show that the P3HT–TiO_2 nanorod hybrid can act as a promising material for future low cost, environmentally friendly, polymer photovoltaic device applications.

Acknowledgements

This work is supported by National Science Council, Taiwan (Project No. NSC95-3114-P-002-003-MY3) and the US Airforce project (AOARD 074-014). The authors would also like to thank Dr Cheng-Hsuan Chen for providing the TEM images.

References

1 W. U. Huynh, J. J. Dittmer and A. P. Alivisatos, *Science*, 2002, **295**, 2425.
2 W. Ma, C. Yang, X. Gong, K. Lee and A. J. Heeger, *Adv. Funct. Mater.*, 2005, **15**, 1617.
3 R. H. Friend, G. J. Denton, J. J. M. Halls, N. T. Harrison, A. B. Holmes, A. Kohler, A. Lux, S. C. Moratti, K. Pichler, N. Tessler, K. Towns and H. F. Wittmann, *Solid State Commun.*, 1997, **102**, 249.
4 T. J. Savenije, J. M. Warman and A. Goossens, *Chem. Phys. Lett.*, 1998, **287**, 148.
5 A. C. Arango, L. R. Johnson, V. N. Bliznyuk, Z. Schlesinger, S. A. Carter and H. H. Horhold, *Adv. Mater.*, 2000, **12**, 1689.
6 N. C. Greenham, X. Peng and A. P. Alivisatos, *Phys. Rev. B*, 1996, **54**, 17628.
7 S. Zhang, P. W. Cyr, S. A. McDonald, G. Konstantatos and E. H. Sargent, *Appl. Phys. Lett.*, 2005, **87**, 233101.
8 C. Y. Kwong, W. C. H. Choy, A. B. Djurišic, P. C. Chui, K. W. Cheng and W. K. Chan, *Nanotechnology*, 2004, **15**, 1156.
9 T. W. Zeng, Y. Y. Lin, H. H. Lo, C. W. Chen, C. H. Chen, S. C. Liou, H. Y. Huang and W. F. Su, *Nanotechnology*, 2006, **15**, 5387.
10 K. M. Coakley and M. D. McGehee, *Appl. Phys. Lett.*, 2003, **83**, 3380.
11 Ravirajan, S. A. Haque, J. R. Durrant, D. D. C. Bradley and J. Nelson, *Adv. Funct. Mater.*, 2005, **15**, 609.
12 W. J. E. Beek, M. M. Wienk and R. A. J. Janssen, *Adv. Mater.*, 2004, **16**, 1009.
13 P. D. Cozzoli, A. Kornowski and H. Weller, *J. Am. Chem. Soc.*, 2003, **125**, 14539.
14 S. A. Choulis, Y. Kim, J. Nelson, D. D. C. Bradley, M. Giles, M. Shkunov and I. McCulloch, *Appl. Phys. Lett.*, 2004, **85**, 3890.
15 H. Bässler, *Phys. Status Solidi B*, 1993, **175**, 15.
16 S. M. Tuladhar, D. Poplavskyy, S. A. Choulis, J. R. Durrant and D. D. C. Bradley, *Adv. Funct. Mater.*, 2005, **15**, 1171.
17 G. Li, V. Shrotriya, J. Huang, Y. Yao, T. Moriarty, K. Emery and Y. Yang, *Nat. Mater.*, 2005, **4**, 864.
18 W. U. Huynh, J. J. Dittmer, W. C. Libby, G. L. Whiting and A. P. Alivisatos, *Adv. Funct. Mater.*, 2003, **13**, 73.
19 Y. Y. Lin, C. W. Chen, T. H. Chu, W. F. Su, C. C. Lin, C. H. Ku, J. J. Wu and C. H. Chen, *J. Mater. Chem.*, 2007, **17**, 4571.
20 Y. Liu, S. R. Scully, M. D. McGehee, J. Liu, C. K. Luscombe, J. M. J. Frechet, S. E. Shaheen and D. S. Giniey, *J. Phys. Chem.*, 2006, **110**, 3257.
21 H. J. Snaith, A. J. Moule, C. Klein, K. Meerholz, R. H. Friend and M. Graetzel, *Nano Lett.*, 2007, **7**, 3372.